Journal of Sound and Vibration (1998) **213**(3), 511–535

VIBRATIONAL ENERGY FLOWS BETWEEN PLATES WITH COMPLIANT AND DISSIPATIVE COUPLINGS

M. BESHARA

Department of Engineering Science, University of Oxford, Parks Road, Oxford, OX1 3PJ, England

AND

A. J. KEANE

Department of Mechanical Engineering, University of Southampton, Highfield, Southampton, SO17 1BJ, England

(*Received* 13 *January* 1997, *and in final form* 19 *January* 1998)

In this work, the transmission of energy through a compliant and dissipative joint between two thin rectangular plates is investigated using a receptance approach. Exact formulae for the spectral density of the energy flow through the joint, the energy dissipated at the joint, the power input by the external excitation and the vibrational energies of the two plates are established when the plates are subject to random ergodic forcing. The more general case of a row of plates which are simply supported along the two longitudinal edges and coupled through compliant and dissipative joints is also investigated. The aim of this study is to examine the effect of joint damping and compliance on the magnitudes of energy flows through the joints and energy levels of the plates. Interest is focused on the energy dissipation at the joints and the conditions for which it is maximised.

1. INTRODUCTION

Considerable attention has been focused on the dynamic behaviour of rectangular plates coupled together. Such configurations can be found in many real structures such as aircraft [1] or buildings [2]. The solution of the problem of energy flow between two plates coupled together has been reported in the literature for many configurations and using various analytical methods. Methods based on semi-infinite models with various types of joints between the plates have been described by Craven and Gibbs [3], Petersson *et al.* [4] and Cremer *et al.* [5]. The displacements in such models are expressed as waves propagating in the structure. However, they are not easily applied to systems with multiple joints without recourse to some kind of ray tracing approach.

Coupled plates have also been analysed based on models of finite-sized plates using several approaches. Guyader *et al.* [6] and Shen and Gibbs [7] used a theoretical method based on finding the global modes of the coupled structure and vibrational energy flows were then calculated based on a modal approach using these global modes. This method becomes very cumbersome for large numbers of plates coupled together. An alternative method which can also be used in some cases is the dynamic stiffness method which has been applied by Langley [8] to calculate the transverse response of a row of coupled plates subject to an acoustic pressure field. The solution is restricted to the case when two opposing edges are simply supported so that the problem can be reduced from second to first order. The dynamic stiffness matrix of one uncoupled plate can then be derived and

0022–460X/98/230511 + 25 $25.00/0/sv981521

using standard assembly techniques, the dynamic stiffness matrix for the whole structure produced. The degrees of freedom in this method are the deflections at the joints. This approach was also used by Bercin and Langley [9] to study the in-plane vibrations of similar plate structures. Other methods reported in the literature include the mobility approach adopted by Cuschieri [10, 11] to calculate energy flow through "L" shaped finite plates, as well as various numerical solutions based on finite element analyses; see for example Simmons [12]. FE methods are, however, not suitable for the prediction of vibrational energy flow at higher frequencies.

Another method which is extensively reported in the literature is the receptance approach. This was used by Azimi *et al.* [13] to find the mode shapes and natural frequencies for the free vibrations of rectangular plates coupled together. Dimitriadis and Pierce [14] used this method to gain an exact solution for the energy flow between two plates coupled together. Fredo [15] used the method for the analysis of energy flows in three thin rectangular plates connected along two simply supported joints. Kim *et al.* [16] extended the method for a general situation such that there are no limitations on the number of plates connected or the junction type. The receptance method is similar to the dynamic stiffness method in that it also finds the solution in terms of the characteristics of the uncoupled plates. However, the degrees of freedom in this approach are the coupling forces at the joints rather than the displacements used in the dynamic stiffness method. These unknown coupling forces are calculated by utilizing the compatibility conditions at each joint. In this method, as in all exact approaches, the solutions reported in the literature are restriced to the case of plates simply supported along two opposite edges.

In this work, the examples considered are again restricted to having simply supported edges along two opposite sides but now they are taken to be coupled together by compliant and dissipative joints, as little attention seems to have been focused on this case. First, the case of just two simply supported plates coupled together by a compliant and dissipative joint is considered, which is the simplest model possible. Exact solutions for the energy flows and energy levels are found for the two cases of point and "rain-on-the-roof" forcing. The results obtained are compared to those for the related one-dimensional case which has been discussed before [17]. Next, the more general case of multiple rectangular plates coupled together by compliant and dissipative joints is cast in a matrix form and a general solution for the various energy resources derived. The same results can be derived by the dynamic stiffness method but the number of degrees of freedom in the receptance method is less than that of the equivalent dynamic stiffness method for the case of compliant joints. Numerical examples are provided which illustrate the effect of damping in the coupling on the characteristics of the energy flows and energy levels of the plates. The conditions for which the energy dissipated at the joints is maximised are also discussed.

2. THEORY

Consider a system which consists of two rectangular plates coupled together along one compliant and dissipative joint as shown in Figure 1. The plates are assumed to be thin, isotropic and homogeneous so that the classical thin plates theory holds. Each plate n has mass per unit area ρ_n, viscous damping coefficient c_n and bending rigidity D_n given by

$$D_n = \frac{E_n h_n^3}{12(1 - \nu_n^2)} \quad n = 1, 2. \tag{1}$$

Note that other damping models could be assumed and somewhat different results achieved. Here E_n is the elastic modulus and ν_n the Poisson ratio of the material. The dimensions of plate n are L_{xn} and L_y so that the two plates have the same length along

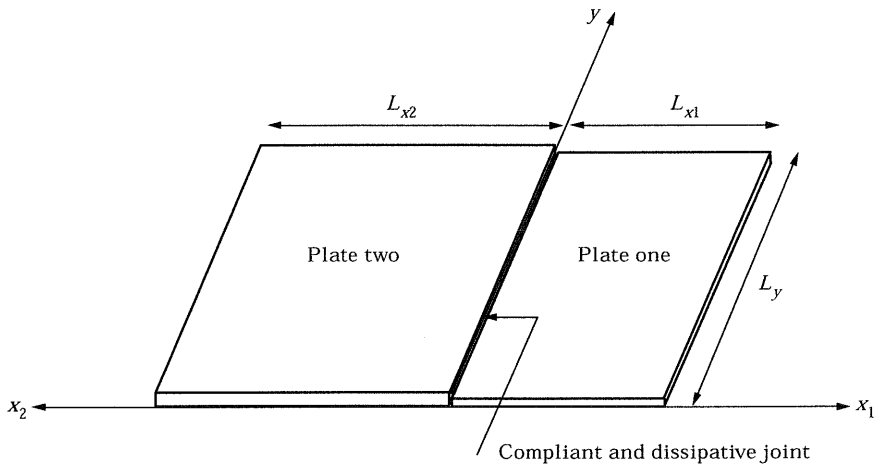

Figure 1. Two simply supported plates coupled together.

the joint, which is assumed to have a constant complex rotational stiffness $\Omega = K + i\gamma\omega$, per unit of length. First, the two plates are assumed to be simply supported along all edges so that energy is transmitted through the joint by moments only and the modal components in the y direction are identical for both plates (note, this kind of coupling implies that the plates may be at arbitrary angles to each other). The two plates are excited by arbitrary forces $f_n(x_n, y, \omega)$ which are taken to be random, stationary and ergodic processes. The resulting displacements have the same properties because the system is linear.

The compatibility conditions at the joint require that the total rotation of plate n at the coupled edge, denoted by $\theta_n(0, y, \omega)$, is equal to the rotation due to the external forces applied to the uncoupled plate $\theta_n^0(0, y, \omega)$ plus the rotation due to the coupling moments which act along the edge $\theta_{nc}(0, y, \omega)$. These conditions can be written as follows

$$\theta_n(0, y, \omega) = \theta_n^0(0, y, \omega) + \theta_{nc}(0, y, \omega) \qquad n = 1, 2. \tag{2}$$

The rotation $\theta_n(0, y, \omega)$ can be written in a series form in terms of the modes of the uncoupled plate as follows

$$\theta_n(0, y, \omega) = \sum_i \sum_j W_{n,ij}(\omega) \Psi'_{n,i}(0) \Phi_j(y) \tag{3}$$

where $\Psi_{n,i}(x_n)$ is the ith mode shape in the $x_n$dire ction, $\Phi_j(y)$ is the jth modal component in the y direction (which is the same for both plates because they have identical boundary conditions along the x_1 and x_2 directions) and the prime indicates differentiation with respect to x. These mode shapes are independent in the x and y directions when the plate is simply supported along two opposing edges. For the case of uniform plates simply supported along all edges considered here, the mode shapes are sinusoidal. The orthogonality condition requires that

$$\int_0^{L_{xn}} \int_0^{L_y} \Psi_i(x_n) \Psi_k(x_n) \Phi_j(y) \Phi_r(y) \, dx_n \, dy = \frac{a_n}{4} \delta_{ik} \delta_{jr}, \tag{4}$$

where a_n is the area of the nth plate. Also the modal components in the y direction satisfy the orthogonality conditions such that

$$\int_0^{L_y} \Phi_j(y)\Phi_r(y)\,dy = \frac{L}{2}\delta_r. \tag{5}$$

The modal component of the Fourier transform of transverse displacement of plate n, $W_{n,ij}(\omega)$, is then given by

$$W_{n,ij}(\omega) = \frac{4}{m_n}\int_0^{L_{xn}}\int_0^{L_y} v_n(x, y, \omega)\Psi_i(x_n)\Phi_j(y)\,dx_n\,dy, \tag{6}$$

where m_n is the total mass of plate n. Based on modal analysis of the plates, the rotation at any point of the coupled edge due to the external forces alone (i.e., when the plate is uncoupled) may be given as an expansion in terms of the mode shapes of the plate by

$$\theta_n^0(0, y, \omega) = \sum_i \sum_j \frac{F_{n,ij}(\omega)\Psi'_{n,i}(0)\Phi_j(y)}{m_n/4H_{n,ij}(\omega)} = \sum_j \theta^0_{n,j}(0, \omega)\Phi_j(y), \tag{7}$$

where

$$\theta^0_{n,j}(0, \omega) = \sum_j \frac{F_{n,ij}(\omega)\Psi'_{n,i}(0)}{m_n/4H_{n,ij}(\omega)}. \tag{8}$$

$F_{n,ij}(\omega)$ is the modal component of the external forcing and is given by

$$F_{n,ij}(\omega) = \int_0^{L_{xn}}\int_0^{L_y} f_n(x_n, y, \omega)\Psi_i(x_n)\Phi_j(y)\,dx_n\,dy \tag{9}$$

and $H_{n,ij}(\omega)$ is the frequency response function of mode ij of plate n which yields the modal displacement due to a modal force and is given by

$$H_{n,ij}(\omega) = \omega^2_{n,ij} - \omega^2 - ic_n\omega, \tag{10}$$

where $\omega_{n,ij}$ is a natural frequency of plate n.

The coupling moment along the edge of plate one arises due to the relative rotation between the two sides of the joint and is defined at any point along the y-axis by

$$M_{1c}(y, \omega) = \Omega\left\{\sum_r \sum_j W_{2,rj}(\omega)\Psi'_{2,r}(0)\Phi_j(y) - \sum_i \sum_j W_{1,ij}(\omega)\Psi'_{1,i}(0)\Phi_j(y)\right\}\delta'(x_1 - 0). \tag{11}$$

Here δ' is the first derivative of the delta function with respect to its argument. This last equation can be written as

$$M_{1c}(y, \omega) = \sum_j \Omega(\theta_{2,j}(0, \omega) - \theta_{1,j}(0, \omega))\Phi_j(y)\delta'(x_1 - 0). \tag{12}$$

As shown in the above equation, the coupling moment which acts along the joint is written as an expansion in terms of the modal components in the y direction, which are sinusoidal in the case considered here. $\theta_{1,j}(0, \omega)$ and $\theta_{2,j}(0, \omega)$ are the jth components of modal expansions of the rotation at the common edge of plates one and two, respectively, along

the y-axis. The coupling moment which acts on the second plate at the common edge has the same amplitude but is in the opposite direction. Utilizing modal analysis of the plates, it can be shown that a moment distributed along an edge of plate n which has a distribution shape along the y-axis as defined in equation (12) gives rise to rotation of the edge given by

$$\theta_{n,c}(0, y, \omega) = \sum_i \sum_j \frac{L_y/2\Psi'^2_{n,i}(0)}{m_n/4H_{n,ij}(\omega)} \Omega(\theta_{2,j}(0, \omega) - \theta_{1,j}(0, \omega))\Phi_j(y). \tag{13}$$

This can also be written as

$$\theta_{n,c}(0, y, \omega) = \sum_j G_{n,j00}(0, 0, \omega)\Omega(\theta_{2,j}(0, \omega) - \theta_{1,j}(0, \omega))\Phi_j(y). \tag{14}$$

Here $G_{n,j\theta\theta}(x, x_0, \omega)$ is the Green function which gives the jth component of rotation at the point x of plate n, denoted by $\theta_{n,j}(x, \omega)$, due to unit jth component of a modal expansion along the y-axis of moment $M_{n,j}(x, \omega)$ applied at point x_0 and is given by

$$G_{n,j00}(x, x_0, \omega) = \sum_i \frac{\Psi'_{n,i}(x)\Psi'_{n,i}(x_0)}{\rho_n L_{x_n}/2H_{n,ij}(\omega)}. \tag{15}$$

The main equations can thus be rewritten as follows

$$\sum_j \theta_{1,j}(0, \omega)\Phi_j(y) = \sum_j \theta^0_{1,j}(0, \omega)\Phi_j(y) + G_{1,j00}(0, 0, \omega)\Omega(\theta_{2,j}(0, \omega) - \theta_{1,j}(0, \omega))\Phi_j(y) \tag{16a}$$

and

$$\sum_j \theta_{2,j}(0, \omega)\Phi_j(y) = \sum_j \theta^0_{2,j}(0, \omega)\Phi_j(y) + G_{2,j00}(0, 0, \omega)\Omega(\theta_{1,j}(0, \omega) - \theta_{2,j}(0, \omega))\Phi_j(y). \tag{16b}$$

Multiplying both equations by any $\Phi_j(y)$ and taking the integral over L_y, these last two expressions can be written as

$$\theta_{1,j}(0, \omega) = \theta^0_{1,j}(0, \omega) + G_{1,j00}(0, 0, \omega)\Omega(\theta_{2,j}(0, \omega) - \theta_{1,j}(0, \omega)) \tag{17a}$$

and

$$\theta_{2,j}(0, \omega) = \theta^0_{2,j}(0, \omega) + G_{2,j00}(0, 0, \omega)\Omega(\theta_{1,j}(0, \omega) - \theta_{2,j}(0, \omega)). \tag{17b}$$

Solving these equations together gives the jth modal components of rotation along the common edge as

$$\theta_{1,j}(0, \omega) = \theta^0_{1,j}(0, \omega) + \frac{\Omega}{\Delta_j(\omega)} G_{1,j00}(0, 0, \omega)(\theta^0_{2,j}(0, \omega) - \theta^0_{1,j}(0, \omega)) \tag{18a}$$

and

$$\theta_{2,j}(0, \omega) = \theta^0_{2,j}(0, \omega) + \frac{\Omega}{\Delta_j(\omega)} G_{2,j00}(0, 0, \omega)(\theta^0_{1,j}(0, \omega) - \theta^0_{2,j}(0, \omega)), \tag{18b}$$

where

$$\Delta_j(\omega) = 1 + \Omega(G_{1,j_{00}}(0, 0, \omega) + G_{2,j_{00}}(0, 0, \omega)). \tag{19}$$

It is clear from the above analysis that the double summations implied in equations (16) have been reduced to single summations over the modes in the x direction of both plates. The problem is thus transformed from one in two dimensions to a one-dimensional problem in the variable x.

It is seen that the modal components in the y direction act independently of one another, and this means that the jth modal rotation $\theta_{n,j}(0, \omega)$ depends only on the characteristics of mode j of the two plates (i.e., their corresponding mode shapes and natural frequencies) and that the other modal components in the y direction have no effect. This is a direct result of the fact that the two plates have identical mode shapes in the y direction.

It follows that the joint in this case couples each mode j in the y direction of the first plate with its counterpart in the second plate. Each mode j of plates one and two can thus be thought of as being those of beams of length L_{x_1} and L_{x_2}, respectively, with mode shapes and natural frequencies of those of mode $j$in plates one and two, coupled by a joint which has a complex stiffness Ω and subject to modal forces $F_{1,j}(x, \omega)$ and $F_{2,j}(x, \omega)$ defined as

$$F_{n,j}(x, \omega) = \frac{2}{L_y}\int_0^{L_y} f_n(x, y, \omega)\Phi(y)\,\mathrm{d}y \qquad n = 1, 2. \tag{20}$$

When the compatibility conditions are applied at the coupling boundary point of these two beams, equations (17) are recovered.

3. ENERGY FLOWS AND ENERGY DISSIPATION AT THE JOINT

The spectral density of the energy flow from plate one to plate two through the joint is given by

$$\Pi_{12}^{I}(\omega) = \int_0^{L_y} \mathrm{i}\Omega\omega S_{\theta_1\theta_2}(y, \omega)\,\mathrm{d}y + \int_0^{L_y} \gamma\omega^2 S_{\theta_1\theta_1}(y, \omega)\,\mathrm{d}y, \tag{21}$$

where $S_{\theta_1\theta_2}(y, \omega)$ is the cross spectral density of the rotation of plates one and two at the common edge and for a stationary random process is taken to be

$$S_{\theta_1\theta_2}(y, \omega) = \lim_{T\to\infty}\frac{2\pi}{T}\theta_1^*(0, y, \omega)\theta_2(0, y, \omega). \tag{22}$$

Substituting in terms of modal expansions along the y-axis gives

$$\Pi_{12}^{I}(\omega) = \mathrm{i}\Omega\omega\lim_{T\to\infty}\frac{2\pi}{T}\int_0^{L_y}\sum_j\sum_k \theta_{1,j}^*(\omega)\theta_{2,k}(\omega)\Phi_j(y)\Phi_k(y)\,\mathrm{d}y$$

$$+ \gamma\omega^2\lim_{T\to\infty}\frac{2\pi}{T}\int_0^{L_y}\sum_j\sum_k \theta_{1,j}^*(\omega)\theta_{1,k}(\omega)\Phi_j(y)\Phi_k(y)\,\mathrm{d}y. \tag{23}$$

Introducing the orthogonality conditions, the last expression reduces to

$$\Pi_{12}^{l}(\omega) = \mathrm{i}\Omega\omega L_y/2 \lim_{T\to\infty} \frac{2\pi}{T} \sum_j \theta_{1,j}^{*}(\omega)\theta_{2,j}(\omega) + \gamma\omega^2 L_y/2 \lim_{T\to\infty} \frac{2\pi}{T} \sum_j |\theta_{1,j}(\omega)|^2, \quad (24)$$

so that the energy flow from plate one to plate two can be written as an infinite sum over the modal components in the y direction as

$$\Pi_{12}^{l}(\omega) = \sum_j (\mathrm{i}\Omega L_y/2\omega S_{\theta_{1,j}\theta_{2,j}}(\omega) + \gamma L_y/2\omega^2 S_{\theta_{1,j}\theta_{2,j}}(\omega)) = \sum_j L_y/2\Pi_{12,j}^{l}(\omega). \quad (25)$$

It may be seen from the above equation that there is no flow of energy from mode j of the first plate to a different mode k of the second plate. This is a direct result of the fact that the modes of the two plates in the y direction are identical and orthogonal. Therefore, the energy flow is the sum of the energy flow from mode j in the first plate to its counterpart in the second plate taken over all the modes in the y direction multiplied by a factor of $L_y/2$ which results from the integration of energy flow over the lengthof the joint. As has already been mentioned, the energy flow due to one individual mode is analogous to the energy flow between two simply supported beams coupled through a rotational spring and damper.

To proceed with the analysis, an exact expression for the jth component of the energy flow is recovered. First the expression for the cross spectral density $S_{\theta_{1,j}\theta_{2,j}}(\omega)$ is written as

$$S_{\theta_{1,j}\theta_{2,j}}(\omega) = \lim_{T\to\infty} \frac{2\pi}{T} \theta_{1,j}^{*}(\omega)\theta_{2,j}(\omega). \quad (26)$$

Next, substituting the expressions for $\theta_{1,j}(\omega)$ and $\theta_{2,j}(\omega)$ from equations (18) and assuming that the forces acting on the two plates are incoherent, so that the cross spectral density $S_{\theta_{1,j},\theta_{2,j}}(\omega)$ becomes

$$S_{\theta_{1,j}\theta_{2,j}}(\omega) = \frac{\Omega G_{2,j_{00}}(0,0,\omega) + |\Omega G_{2,j_{00}}(0,0,\omega)|^2}{|\Delta_j(\omega)|^2} S_{\theta_{1,j}^0\theta_{2,j}^0}(\omega)$$

$$+ \frac{\Omega^* G_{1,j_{00}}(0,0,\omega) + |\Omega G_{1,j_{00}}(0,0,\omega)|^2}{|\Delta_j(\omega)|^2} S_{\theta_{2,j}^0\theta_{2,j}^0}(\omega). \quad (27)$$

Incoherence is assumed here, in common with most published work on energy flow, since this makes the analysis considerably simpler and also reflects the common situation in engineering problems where the noise sources affecting different parts of a structure are, in practice, often incoherent.

Proceeding in an entirely similar fashion, the spectral density $S_{\theta_{1,j}\theta_{1,j}}(\omega)$ is given by

$$S_{\theta_{1,j}\theta_{1,j}}(\omega) = \frac{|1 + \Omega G_{2,j_{00}}(0,0,\omega)|^2}{|\Delta_j(\omega)|^2} S_{\theta_{1,j}^0\theta_{1,j}^0}(\omega) + \frac{|\Omega G_{1,j_{00}}(0,0,\omega)|^2}{|\Delta_j(\omega)|^2} S_{\theta_{2,j}^0\theta_{2,j}^0}(\omega). \quad (28)$$

The jth component of the energy flow thus becomes

$$\Pi^{l}_{12,j}(\omega) = \mathrm{i}\Omega\omega L_y/2\left(\frac{\Omega G_{2,j_{00}}(0,0,\omega) + |\Omega G_{2,j_{00}}(0,0,\omega)|^2}{|\Delta_j(\omega)|^2} S_{\theta^0_{1,j}\theta^0_{1,j}}(\omega)\right.$$

$$\left. + \frac{\Omega^* G_{1,j_{00}}(0,0,\omega) + |\Omega G_{1,j_{00}}(0,0,\omega)|^2}{|\Delta_j(\omega)|^2} S_{\theta^0_{2,j}\theta^0_{2,j}}(\omega)\right)$$

$$+ \gamma\omega^2 L_y/2\left(\frac{|1 + \Omega G_{2,j_{00}}(0,0,\omega)|^2}{|\Delta_j(\omega)|^2} S_{\theta^0_{1,j}\theta^0_{1,j}}(\omega)\right.$$

$$\left. + \frac{|\Omega G_{1,j_{00}}(0,0,\omega)|^2}{|\Delta_j(\omega)|^2} S_{\theta^0_{2,j}\theta^0_{2,j}}(\omega)\right). \tag{29}$$

In order to obtain the final expression for the energy flow, only the real part of the last expression needs to be considered and, after the necessary mathematical manipulations, the modal component of the energy flow from plate one to plate two is found to be given by

$$\Pi^{l}_{12,j}(\omega) = \frac{-\omega|\Omega|^2 L_y/2}{|\Delta_j(\omega)|^2} \operatorname{Im}\left\{\sum_r \frac{\Psi'^2_{2,r}(0)}{L_{x_2}/2H_{2,rj}(\omega)}\right\} S_{\theta^0_{1,j}\theta^0_{1,j}}(\omega) + \frac{\gamma\omega^2 L_y/2}{|\Delta_j(\omega)|^2} S_{\theta^0_{1,j}\theta^0_{1,j}}(\omega)$$

$$+ \frac{\omega|\Omega|^2 L_y/2}{|\Delta_j(\omega)|^2} \operatorname{Im}\left\{\sum_i \frac{\Psi'^2_{1,i}(0)}{L_{x_1}/2H_{1,ij}(\omega)}\right\} S_{\theta^0_{2,j}\theta^0_{2,j}}(\omega). \tag{30}$$

The spectral density of the modal rotation of plate n along the common edge is written in terms of the spectral density of the modal forces as follows

$$S_{\theta^0_{n,j}\theta^0_{n,j}} = \sum_i \sum_k \frac{\Psi'_{n,i}(0)\Psi'_{n,k}(0)}{(m_n/4)^2 H^*_{n,ij}(\omega) H_{n,kj}(\omega)} S_{F_{n,ij}F_{n,kj}}(\omega) \qquad n = 1, 2 \tag{31}$$

so that the expression for the energy flow becomes

$$\Pi^{l}_{12,j}(\omega) = \left[\frac{-\omega|\Omega|^2 L_y/2}{|\Delta_j(\omega)|^2} \operatorname{Im}\left\{\sum_r \frac{\Psi'^2_{2,r}(0)}{L_{x_2}/2H_{2,rj}(\omega)}\right\} + \frac{\gamma\omega^2 L_y/2}{|\Delta_j(\omega)|^2}\right]$$

$$\times \sum_i \sum_k \frac{\Psi'_{1,i}(0)\Psi'_{1,k}(0)}{(m_1/4)^2 H^*_{1,ij}(\omega) H_{1,kj}(\omega)} S_{F_{1,ij}F_{1,kj}}(\omega) + \frac{\omega|\Omega|^2 L_y/2}{|\Delta_j(\omega)|^2}$$

$$\times \operatorname{Im}\left\{\sum_i \frac{\Psi'^2_{1,i}(0)}{L_{x_i}/2H_{1,ij}(\omega)}\right\} \sum_r \sum_m \frac{\Psi'_{2,r}(0)\Psi'_{2,m}(0)}{(m_2/4)^2 H^*_{2,rj}(\omega) H_{2,mj}(\omega)} S_{F_{2,rj}F_{2,mj}}(\omega). \tag{32}$$

The total energy flow is then calculated from equation (25). The expression for the energy flow from plate two to plate one is derived similarly. Lastly, the energy dissipated at the joint can be recovered from the energy balance at the joint. It is given by

$$\Pi_{DC}(\omega) = \sum_j \Pi_{DC,j}(\omega), \tag{33}$$

where $\Pi_{DC,j}(\omega)$ is the sum of $\Pi^{l}_{12,j}(\omega)$ and $\Pi^{l}_{21,j}(\omega)$ and is given by

$$\Pi_{DC,j}(\omega) = \frac{\gamma\omega^2 L_y/2}{|\Delta_j(\omega)|^2}\sum_i \sum_k \frac{\Psi'_{1,i}(0)\Psi'_{1,k}(0)}{(m_1/4)^2 H^*_{1,ij}(\omega)H_{1,kj}(\omega)} S_{F_{1,ij}F_{1,kj}}(\omega)$$

$$+ \frac{\gamma\omega^2 L_y/2}{|\Delta_j(\omega)|^2}\sum_r \sum_m \frac{\Psi'_{2,r}(0)\Psi'_{2,m}(0)}{(m_2/4)^2 H^*_{2,rj}(\omega)H_{2,mj}(\omega)} S_{F_{2,rj}F_{2,mj}}(\omega). \tag{34}$$

4. INPUT POWER

The spectral density of the input power due to a vertical force applied to plate one is calculated from the product of force and velocity at the point of its application and is given by

$$\Pi_{IN,1}(\omega) = -i\omega \lim_{T\to\infty}\frac{2\pi}{T}\int_0^{L_{x_1}}\int_0^{L_y} v_1^*(x_1, y, \omega) f_1(x_1, y, \omega)\,dx_1\,dy$$

$$= -i\omega \lim_{T\to\infty}\frac{2\pi}{T}\sum_i\sum_j W^*_{1,ij}(\omega)F_{1,ij}(\omega). \tag{35}$$

Substituting $W_{1,ij}(\omega)$ by its value in terms of the modal forcing components deduced from equation (18), this can be written as

$$\Pi_{IN,1}(\omega) = -i\omega \lim_{T\to\infty}\frac{2\pi}{T}\left\{ F_{1,ij}(\omega) \times \left[\sum_i\sum_j \frac{F^*_{1,ij}(\omega) + \dfrac{L_y/2\Omega^*\Psi'_{1,i}(0)}{\Delta_j^*(\omega)}\left[\sum_k \dfrac{F^*_{2,kj}(\omega)\Psi'_{2,k}(0)}{m_2/4H^*_{2,kj}(\omega)} - \sum_m \dfrac{F^*_{1,mj}(\omega)\Psi'_{1,m}(0)}{m_1/4H^*_{1,mj}(\omega)}\right]}{m_1/4H^*_{1,ij}(\omega)}\right]\right\}. \tag{36}$$

Since the forces acting on the two plates are incoherent, then $S_{F_{2,kj}F_{1,ij}}(\omega)$ is zero, and this last equation reduces to

$$\Pi_{IN,1}(\omega) = -i\omega\sum_i\sum_j \frac{S_{F_{1,ij}F_{1,ij}}(\omega)}{m_1/4H^*_{1,ij}(\omega)} + \frac{i\omega L_y/2\Omega^*}{(m_1/4)^2}\sum_i\sum_j\sum_m \frac{\Psi'_{1,i}(0)\Psi'_{1,m}(0)S_{F_{1,mj}F_{1,ij}}(\omega)}{H^*_{1,ij}(\omega)H^*_{1,mj}(\omega)\Delta_j^*(\omega)}. \tag{37}$$

Taking only the real part, the expression for the spectral density of the input power to the first plate is written as

$$\Pi_{IN,1}(\omega) = \frac{\omega}{m_1/4}\sum_i\sum_j \mathrm{Im}\left\{\frac{1}{H^*_{1,ij}(\omega)}\right\}S_{F_{1,ij}F_{1,ij}}(\omega)$$

$$+ \frac{\omega L_y/2}{(m_1/4)^2}\sum_i\sum_j\sum_m \mathrm{Im}\left\{\frac{\Psi'_{1,i}(0)\Psi'_{1,m}(0)\Omega}{H_{1,ij}(\omega)H_{1,mj}(\omega)\Delta_j(\omega)}\right\}S_{F_{1,mj}F_{1,ij}}(\omega). \tag{38}$$

The expression for the input power to plate two can be derived similarly.

5. TWO FORCING MODELS

To proceed further, the expressions for the various energy flows and energy levels are deduced for the two special cases of point and "rain-on-the-roof" driving. The reason for choosing these two models is that both give rise to modal forcing spectral densities which are separable in space and frequency. Moreover, both have simple physical interpretations, i.e., localized or distributed but uncorrelated excitation. The spectral density of the modal force is given by

$$S_{F_{n,ij}F_{n,kj}}(\omega) = \int_0^{L_{xn}}\int_0^{L_{xn}}\int_0^{L_y}\int_0^{L_y} S_{F_nF_n}(\omega, x_n, \hat{x}_n, y, \hat{y})\Psi_{n,i}(x_n)\Psi_{n,k}(\hat{x}_n)\Phi_j(y)\Phi_j(\hat{y})\,dx_n\,d\hat{x}_n\,dy\,d\hat{y} \tag{39}$$

where $\hat{x}_n$ and $\hat{y}$ are dummy variables.

5.1. POINT DRIVING

In the case of a force applied at a single point x_n^0, y^0 on plate n the spectral density of the driving forces is given by

$$S_{F_nF_n}(\omega, x_n, \hat{x}_n, y, \hat{y}) = S_{F_nF_n}(\omega)\delta(x_n - x_n^0)\delta(\hat{x}_n - x_n^0)\delta(y - y^0)\delta(\hat{y} - y^0), \tag{40}$$

and the spectral density of the modal forces is

$$S_{F_{n,ij}F_{n,kj}}(\omega) = S_{F_nF_n}(\omega)\Psi_{n,i}(x_n^0)\Psi_{k,i}(x_n^0)\Phi_j^2(y^0), \tag{41}$$

and therefore

$$S_{\theta^0_{n,j}\theta^0_{n,j}} = \sum_i\sum_j \frac{\Psi'_{n,i}(0)\Psi'_{n,k}(0)\Psi_{n,i}(x_n^0)\Psi_{n,k}(x_n^0)\Phi_j^2(y^0)}{(m_1/4)^2 H^*_{n,ij}(\omega)H^*_{n,kj}(\omega)} S_{F_nF_n}(\omega). \tag{42}$$

5.2. RAIN-ON-THE-ROOF

In this case the spectral density of the driving forces is given by

$$S_{F_nF_n}(\omega, x_n, \hat{x}_n, y, \hat{y}) = S_{F_nF_n}(\omega)\delta(x_n - \hat{x}_n)\delta(y - \hat{y})\frac{4}{m_n}, \tag{43}$$

and the spectral density of the modal forces is

$$S_{F_{n,ij}F_{n,kj}}(\omega) = S_{F_nF_n}(\omega)\delta_{ik}, \tag{44}$$

so that

$$S_{\theta^0_{n,j}\theta^0_{nj}} = \sum_j \frac{\Psi'^2_{n,i}(0)}{(m_1/4)^2|H_{n,ij}(\omega)|^2} S_{F_nF_n}(\omega). \tag{45}$$

The spectral densities of the energy flows, energy dissipation at the joint and input power due to external forcing can then be recovered when these expressions for the modal forcing spectral densities are substituted into equations (32), (34) and (38) above. Note that in the case of point driving, closed form solutions are available for each jth component of the energy receptances.

6. THE CASE OF UNSUPPORTED JOINTS

In the previous section, the case of two coupled plates simply supported along all edges was discussed in detail. The joint was taken to be supported so that only the bending moments at the joint transfer energy. In this section, a more general case of a row of rectangular plates which are simply supported along the longitudinal edges is considered. The plates have the same width L_y in the y direction so that the modal components in this direction are again identical for all plates. In this case, however, the joints are unsupported so that both the shear forces and moments contribute in the transmission of energy through the structure. The row contains $N+1$ plates with different lengths L_{xn} in the x direction, as shown in Figure 2. In what follows, the quantity $X_j(x, \omega)$ represents the jth component of a modal expansion of the quantity $X(x, y, \omega)$ along the y-axis such that

$$X(x, y, \omega) = \sum_j X_j(x, \omega)\Phi_j(y), \tag{46}$$

where $X(x, y, \omega)$ stands for any dynamic quantity in the following analysis.

Each joint n connects two plates n and $n+1$ at edges B and A, respectively. Let $\{\mathbf{Y}\}_{An,j}$ and $\{\mathbf{Y}\}_{Bn,j}$ be the vector of modal displacements of joint n at edges A and B, and $\{\mathbf{Y}^0\}_{An,j}$ and $\{\mathbf{Y}^0\}_{Bn,j}$ be the modal displacements at edges A and B of joint n due to the external forcing only. The vector of modal displacements at any point (x, y) of plate n is denoted by $\{\mathbf{Y}_{n,j}(x, \omega)\}$. These displacements are defined in the local co-ordinates for each plate. Notice that the in-plane displacements are neglected so that the vector of modal displacements at each point of plate n includes the vertical displacement and rotation about the y-axis, i.e.,

$$\{Y_{n,j}(x, \omega)\} = \begin{Bmatrix} v_{n,j}(x, \omega) \\ \theta_{n,j}(x, \omega) \end{Bmatrix}. \tag{47}$$

The vector of modal displacements at edge A of joint n is thus related to the vector of modal displacements of plate $n+1$ as

$$\{\mathbf{Y}\}_{An,j} = \{Y_{(n+1),j}(0, \omega)\}, \tag{48}$$

while the vector of modal displacements at edge B of joint n is related to the vector of modal displacements of plate n as

$$\{\mathbf{Y}\}_{Bn,j} = \{Y_{n,j}(L_{xn}, \omega)\}. \tag{49}$$

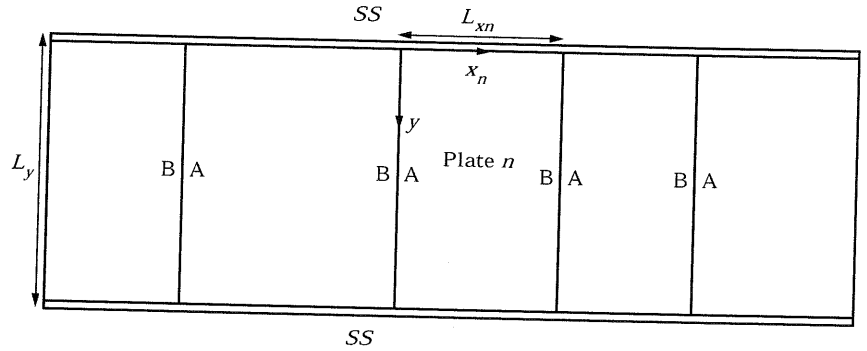

Figure 2. A row of rectangular plates simply supported along their longitudinal edges.

The matrix of Green functions of plate n which relates the vector of the modal displacements $\{\mathbf{Y}_{n,j}(x_1, \omega)\}$ of plate n to the vector of harmonic modal forces $\{\mathbf{F}_{n,j}(x_2, \omega)\}$ is defined as

$$[\mathbf{G}_{n,j}(x_1, x_2, \omega)] = \begin{bmatrix} G_{n,j_{vv}}(x_1, x_2, \omega) & G_{n,j_{v\theta}}(x_1, x_2, \omega) \\ G_{n,j_{\theta v}}(x_1, x_2, \omega) & G_{n,j_{\theta\theta}}(x_1, x_2, \omega) \end{bmatrix}. \tag{50}$$

The functions which constitute the matrix are

$$G_{n,j_{vv}}(x_1, x_2, \omega) = \sum_i \frac{\Psi_{n,i}(x_1)\Psi_{n,i}(x_2)}{\rho_n L_{xn}/2H_{n,ij}(\omega)}, \tag{51a}$$

$$G_{n,j_{v\theta}}(x_1, x_2, \omega) = \sum_i \frac{\Psi_{n,i}(x_1)\Psi'_{n,i}(x_2)}{\rho_n L_{xn}/2H_{n,ij}(\omega)} \tag{51b}$$

and

$$G_{n,j_{\theta\theta}}(x_1, x_2, \omega) = \sum_i \frac{\Psi'_{n,i}(x_1)\Psi'_{n,i}(x_2)}{\rho_n L_{xn}/2H_{n,ij}(\omega)}. \tag{51c}$$

Closed-form solutions for these functions are available. Next the flexibility matrix of plate n which relates the modal displacements at the two edges A, B with the corresponding modal forces is defined as

$$[\mathbf{G}_{n,j}] = \begin{bmatrix} [G_{n,j}]_{AA} & [G_{n,j}]_{AB} \\ [G_{n,j}]_{BA} & [G_{n,j}]_{BB} \end{bmatrix}, \tag{52}$$

where

$$[\mathbf{G}_{n,j}]_{AA} = [G_{n,j}(0, 0, \omega)], \qquad [\mathbf{G}_{n,j}]_{AB} = [G_{n,j}(0, L_{xn}, \omega)], \tag{53a, b}$$

$$[\mathbf{G}_{n,j}]_{BA} = [G_{n,j}(L_{xn}, 0, \omega)], \qquad [\mathbf{G}_{n,j}]_{BB} = [G_{n,j}(L_{xn}, L_{x_n}\omega)]. \tag{53c, d}$$

Writing $[\mathbf{\Omega}]_n$ as the diagonal matrix of the complex stiffness of joint n and $\{\mathbf{\Delta Y}\}_{n,j}$ as the vector of relative displacements between the edges A and B of joint n, then the compatibility conditions for joint n at edge A require that

$$\{\mathbf{Y}\}_{An,j} = \{\mathbf{Y}^0\}_{An,j} - [\mathbf{G}_{(n+1),j}]_{AA}[\mathbf{\Omega}]_n \{\mathbf{\Delta Y}\}_{n,j} + [\mathbf{G}_{(n+1),j}]_{AB}[\mathbf{\Omega}]_{(n+1)} \{\mathbf{\Delta Y}\}_{(n+1),j} \tag{54}$$

and the compatibility conditions for joint n at edge B that

$$\{\mathbf{Y}\}_{Bn,j} = \{\mathbf{Y}^0\}_{Bn,j} - [\mathbf{G}_{n,j}]_{BA}[\mathbf{\Omega}]_{(n-1)} \{\mathbf{\Delta Y}\}_{(n-1),j} + [\mathbf{G}_{n,j}]_{BB}[\mathbf{\Omega}]_n \{\mathbf{\Delta Y}\}_{n,j}. \tag{55}$$

Following similar steps to those given in the previous sections it may be shown that the main equations of the receptance approach can be written for the whole assembled system of plates in the form

$$\{\mathbf{Y}\}_{A,j} = \{\mathbf{Y}^0\}_{A,j} - [\mathbf{A}_j]_A \{\{\mathbf{Y}\}_{A,j} - \{\mathbf{Y}\}_{B,j}\} \tag{56a}$$

and

$$\{\mathbf{Y}\}_{B,j} = \{\mathbf{Y}^0\}_{B,j} + [\mathbf{A}_j]_B \{\{\mathbf{Y}\}_{A,j} - \{\mathbf{Y}_j\}_{B,j}\}. \tag{56b}$$

Here $\{\mathbf{Y}\}_{A,j}$, $\{\mathbf{Y}\}_{B,j}$ are the vectors of modal displacements at the edges A, B of all the joints. The matrices $[\mathbf{A}_j]_A$ and $[\mathbf{A}_j]_B$ are constructed by assembly and given by

$$[\mathbf{A}_j]_A = \begin{bmatrix} [\mathbf{G}_{2,j}]_{AA} & -[\mathbf{G}_{2,j}]_{AB} & (0) & \cdots & [\mathbf{0}] \\ [\mathbf{0}] & [\mathbf{G}_{3,j}]_{AB} & -[\mathbf{G}_{3,j}]_{AB} & \cdots & [\mathbf{0}] \\ [\mathbf{0}] & [\mathbf{0}] & [\mathbf{G}_{4,j}]_{AA} & \cdots & [\mathbf{0}] \\ [\mathbf{0}] & [\mathbf{0}] & [\mathbf{0}] & \cdots & [\mathbf{G}_{N+1,j}]_{AA} \end{bmatrix} [\boldsymbol{\Omega}] \tag{57a}$$

$$[\mathbf{A}_j]_B = \begin{bmatrix} [\mathbf{G}_{1,j}]_{BB} & [\mathbf{0}] & [\mathbf{0}] & \cdots & [\mathbf{0}] \\ -[\mathbf{G}_{2,j}]_{BA} & [\mathbf{G}_{2,j}]_{BB} & [\mathbf{0}] & \cdots & [\mathbf{0}] \\ [\mathbf{0}] & -[\mathbf{G}_{3,j}]_{BA} & [\mathbf{G}_{3,j}]_{BB} & \cdots & [\mathbf{0}] \\ [\mathbf{0}] & [\mathbf{0}] & [\mathbf{0}] & \cdots & [\mathbf{G}_{N,j}]_{BB} \end{bmatrix} [\boldsymbol{\Omega}], \tag{57b}$$

where $[\boldsymbol{\Omega}]$ denotes the diagonal matrix of the complex stiffness of the joints in the assembled system. Equations (56) can now be solved and the expressions for the modal displacements at the edges A, B of the joints recovered. This is similar to the case of multiple beams coupled together which was considered in a previous study [18]. The results for the modal displacements may be recapitulated as follows

$$\{\mathbf{Y}\}_{A,j} = [([\mathbf{I}] + [\mathbf{A}_j]_B) \mid [\mathbf{A}_j]_A] \begin{bmatrix} [\mathbf{D}_j]^{-1} & [\mathbf{0}] \\ [\mathbf{0}] & [\mathbf{D}_j]^{-1} \end{bmatrix} \begin{Bmatrix} \{\mathbf{Y}^0\}_{A,j} \\ \{\mathbf{Y}^0\}_{B,j} \end{Bmatrix}, \tag{58a}$$

$$\{\mathbf{Y}\}_{B,j} = [[\mathbf{A}_j]_B \mid ([\mathbf{I}] + [\mathbf{A}_j]_A)] \begin{bmatrix} [\mathbf{D}_j]^{-1} & [\mathbf{0}] \\ [\mathbf{0}] & [\mathbf{D}_j]^{-1} \end{bmatrix} \begin{Bmatrix} \{\mathbf{Y}^0\}_{A,j} \\ \{\mathbf{Y}^0\}_{B,j} \end{Bmatrix}, \tag{58b}$$

where

$$[\mathbf{D}_j] = [\mathbf{I}] + [\mathbf{A}_j]_A + [\mathbf{A}_j]_B. \tag{59}$$

The displacements at the joints can also be derived using the dynamic stiffness method. However, since the joints in the system considered here are compliant so that the deflections at the two ends of each joint are not equal, the degrees of freedom will be the displacement and rotation about the y-axis at each end of the plate thus making the total number of degrees of freedom for the whole system $4(N+1)$. In the method introduced here, there are only two degrees of freedom at each joint (which are the coupling shear force and moment) so that the total number of degrees of freedom in the proposed method is only $2N$.

7. ENERGY FLOWS AND ENERGY DISSIPATION AT EACH JOINT

The energy flow that leaves plate $n+1$ at edge A is given by

$$\{\Pi\}_{\text{coupA}n}(\omega) = \int_0^{L_y} \mathrm{i}\omega[\boldsymbol{\Omega}]_n \{\mathbf{S}_{Y_{A,n}Y_{B,n}}(y,\omega)\}\,\mathrm{d}y + \int_0^{L_y} \omega^2[\boldsymbol{\gamma}]_n \{\mathbf{S}_{Y_{A,n}Y_{A,n}}(y,\omega)\}\,\mathrm{d}y. \tag{60}$$

Writing $\{\mathbf{Y}\}_{A,n}$ and $\{\mathbf{Y}\}_{B,n}$ as an expansion in terms of the modal components in the y direction, and making use of the orthogonality of the mode shapes, the integrals may be

eliminated and the expression for the energy flow given in terms of modal displacements spectral densities as

$$\{\Pi\}_{\text{coupA}n}(\omega) = \sum_j (L_y/2)\,[i\omega[\boldsymbol{\Omega}]_n \{\mathbf{S}_{Y_{Aj,n}Y_{Bj,n}}(\omega)\} + \omega^2[\boldsymbol{\gamma}]_n \{\mathbf{S}_{Y_{Aj,n}Y_{Aj,n}}(\omega)\}]$$

$$= \sum_j (L_y/2)\{\boldsymbol{\Pi}\}_{\text{coupA}n,j}(\omega). \tag{61}$$

The energy flow is therefore the sum of the energy flow from each mode j to its counterpart and again there is no coupling between the modal components in the y direction. The modal spectral density is written in terms of the modal spectral density of the displacements due to external forcing and is given by the diagonal elements of the product

$$\left[[([\mathbf{I}] + [\mathbf{A}_j]_B) \mid [\mathbf{A}_j]_A]\begin{bmatrix}[\mathbf{D}_j]^{-1} & [\mathbf{0}] \\ [\mathbf{0}] & [\mathbf{D}_j]^{-1}\end{bmatrix}\right]^*_n [\mathbf{S}_{Y^0_{Aj}Y^0_{Bj}}]$$

$$\times\left[\begin{bmatrix}[\mathbf{D}_j]^{-1} & [\mathbf{0}] \\ [\mathbf{0}] & [\mathbf{D}_j]^{-1}\end{bmatrix}^T [[\mathbf{A}_j]_B \mid ([\mathbf{I}] + [\mathbf{A}_j]_A)]^T\right]_n. \tag{62}$$

The matrix of spectral densities $[\mathbf{S}_{Y^0_{Aj}Y^0_{Bj}}(\omega)]$ is related to all the forces acting on the plates. If the external forces acting on the various subsystems are assumed to be uncorrelated and the components of the vector of forces acting on any one subsystem are also uncorrelated then the matrix is diagonal. The following analysis is again restricted to the case when the spectral density of the modal forces is separable in space and frequency. Under these conditions, the matrix $[\mathbf{S}_{Y^0_{Aj}Y^0_{Bj}}(\omega)]$ is written as $[\mathbf{S}_{Y^0_{Aj}Y^0_{Bj}}(\omega)] = \Sigma_n [\mathbf{Q}]_n S_{F_{n,j}F_{n,j}}$ where $[\mathbf{Q}]_n$ contains integrals of Green functions and forces acting on the subsystems. Finally, the energy that flows into edge A of joint n from plate $n+1$ is written as

$$\{\boldsymbol{\Pi}\}_{\text{coupA}n,j} = \sum_k \{\mathbf{H}\}_{Ank,j} S_{F_{k,j}F_{k,j}}, \tag{63}$$

where

$$\{\mathbf{H}\}_{Ank,j} = \text{Re}\Bigg\{i\omega[\boldsymbol{\Omega}]_n\left[[([\mathbf{I}] + [\mathbf{A}_j]_B)^* \mid [\mathbf{A}_j]^*_A]\begin{bmatrix}[\mathbf{D}_j]^{-1} & [\mathbf{0}] \\ [\mathbf{0}] & [\mathbf{D}_j]^{-1}\end{bmatrix}^*\right]_n$$

$$\times [\mathbf{Q}]_k\left[\begin{bmatrix}[\mathbf{D}_j]^{-1} & [\mathbf{0}] \\ [\mathbf{0}] & [\mathbf{D}_j]^{-1}\end{bmatrix}^T [[\mathbf{A}_j]_B \mid ([\mathbf{I}] + [\mathbf{A}_j]_A)]^T\right]_n$$

$$+ [\boldsymbol{\gamma}]_n\,\omega^2\left[[([\mathbf{I}] + [\mathbf{A}_j]_B)^* \mid [\mathbf{A}_j]^*_A]\begin{bmatrix}[\mathbf{D}_j]^{-1} & [\mathbf{0}] \\ [\mathbf{0}] & [\mathbf{D}_j]^{-1}\end{bmatrix}^*\right]_n$$

$$\times [\mathbf{Q}]_k\left[\begin{bmatrix}[\mathbf{D}_j]^{-1} & [\mathbf{0}] \\ [\mathbf{0}] & [\mathbf{D}_j]^{-1}\end{bmatrix}^T [([\mathbf{I}] + [\mathbf{A}_j]_B \mid [\mathbf{A}_j]_A]^T\right]_n\Bigg\} \tag{64}$$

and k is a dummy counter in the summations. These expressions are similar to those which were derived in a previous study for the case of multiple beams coupled together [18].

8. INPUT POWER

The input power to plate n is written in the frequency domain as

$$\{\mathbf{\Pi}\}_{INn} = \mathrm{Re}\left\{\int_0^{L_{xn}}\int_0^{L_y} -i\omega[(\mathbf{Y}_n^*(x,y,\omega)\}\{\mathbf{F}_n(x,y,\omega)\}^T]_{diag}\,dx\,dy\right\}$$

$$= -\omega\,\mathrm{Im}\left\{\int_0^{L_{xn}}\int_0^{L_y}[\{\mathbf{Y}_n(x,y,\omega)\,|\,\{\mathbf{F}_n(x,y,\omega)\}^T]_{diag}\,dx\,dy\right\}. \tag{65}$$

Introducing equation (45), the integration over y may be eliminated and the input power is then given by

$$\{\mathbf{\Pi}\}_{INn} = \sum_j -\psi L_y/2\,\mathrm{Im}\left\{\int_0^{L_{xn}}[\{\mathbf{Y}_{n,j}(x,\omega)\}\{\mathbf{F}_{n,j}(x,\omega)\}^T]_{diag}\,dx\right\}. \tag{66}$$

The input power due to the external forcing alone, without the coupling forces is written as

$$\{\mathbf{\Pi}\}^0_{INn} = \sum_j -\omega\,\mathrm{Im}\left\{\int_0^{L_{xn}}\int_0^{L_{xn}}[\mathbf{G}_{n,j}(x,\hat{x},\omega)]_{diag}\{\mathbf{S}_{F_{nj}F_{nj}}(x,\hat{x},\omega)\}\,dx\,d\hat{x}\right\}. \tag{67}$$

The modal displacement at point x of plate n due to the coupling forces $\{\mathbf{Y}_{nc,j}(x,\omega)\}$ can then be written as

$$\{\mathbf{Y}_{nc,j}(x,\omega)\} = -[\mathbf{G}_{n,j}(x,0,\omega)]\,[\mathbf{\Omega}]_{n-1}\{\Delta\mathbf{Y}\}_{(n-1),j} + [\mathbf{G}_{n,j}(x,L_{xn},\omega)]\,[\mathbf{\Omega}]_n\{\Delta\mathbf{Y}\}_{n,j}. \tag{68}$$

The vector $\{\mathbf{\Delta Y}\}_{n,j}$ is related to the relative displacements due to the external forces alone $\{\Delta\mathbf{Y}^0\}_{n,j}$ by

$$\{\mathbf{\Delta Y}\}_{n,j} = \sum_k [\mathbf{D}]^{-1}_{nm}\{\mathbf{\Delta Y}^0\}_{k,j},$$

(where k is again a dummy counter in the summation) which may be written as

$$\{\mathbf{\Delta Y}\}_{n,j} = \sum_k [\mathbf{D}]^{-1}_{nk}\int_0^{L_{x_{k+1}}}[\mathbf{G}_{(k+1),j}(0,x,\omega)]\{\mathbf{F}_{(k+1),j}(x,\omega))\,dx$$

$$-\int_0^{L_{x_k}}[\mathbf{G}_{k,j}(L_{x_k},x,\omega)]\;\mathbf{F}_{k,j}(x,\omega)\}\,dx], \tag{69}$$

so that the input power due to the coupling forces is given by

$$\{\Pi\}_{INnc} = \sum_j -\omega L_y/2\,\mathrm{Im}\left\{\int_0^{L_{xn}}[\{\mathbf{Y}_{nc,j}(x,\omega)\}\{\mathbf{F}_{n,j}(x,\omega)\}^T]_{diag}\,dx\right\}. \tag{70}$$

Substituting equations (68) and (69) into equation (70) and noting that the forces acting on the various subsystems are uncorrelated and their cross spectral densities are therefore zero, the expression for the input power due to the coupling forces is given by

$$\{\Pi\}_{INnc} = \sum_j \omega L_y /2 \text{ Im} \left\{ \int_0^{L_{xn}} \int_0^{L_{xn}} [[\mathbf{G}_{n,j}(x, 0, \omega)] [\boldsymbol{\Omega}]_{n-1} [\mathbf{D}]^{-1}_{(n-1,n-1)} \right.$$
$$\times [\mathbf{G}_{n,j}(0, \hat{x}, \omega)] [\mathbf{S}_{F_{n,j}F_{n,j}}(x, \hat{x}, \omega)]$$
$$- [\mathbf{G}_{n,j}(x, 0, \omega)] [\boldsymbol{\Omega}]_{n-1} [\mathbf{D}]^{-1}_{(n-1,n)} [\mathbf{G}_{n,j}(L_{xn}, \hat{x}, \omega)] [\mathbf{S}_{F_{n,j}F_{n,j}}(x, \hat{x}, \omega)]$$
$$- [\mathbf{G}_{n,j}(x, L_{xn}, \omega)] [\boldsymbol{\Omega}]_n [\mathbf{D}]^{-1}_{(n,n-1)} [\mathbf{G}_{n,j}(0, \hat{x}, \omega)] [\mathbf{S}_{F_{n,j}F_{n,j}}(x, \hat{x}, \omega)]$$
$$\left. + [\mathbf{G}_{n,j}(x, L_{xn}, \omega)] [\boldsymbol{\Omega}]_n [\mathbf{D}]^{-1}_{(n,n)} [\mathbf{G}_{n,j}(L_{xn}, \hat{x}, \omega)] [\mathbf{S}_{F_{n,j}F_{n,j}}(x, \hat{x}, \omega)]]_{diag} \, dx \, d\hat{x} \right\} \tag{71}$$

The total input power to plate n is then the sum of the two components given by equations (67) and (71) above.

9. NUMERICAL EXAMPLES

9.1. TWO PLATES

Consider two simply supported plates coupled together. The properties of the two plates have been chosen arbitrarily for the purposes of illustration and are given in Table 1. The joint between the two plates comprises a stiffness K and a damping strength γ, both per unit length of plate. Plate one is driven by point forcing. The aim is to study the effects of variation in the coupling strength on the various energy receptances derived in the previous sections.

The power input to the first plate may be divided into three parts: some of it will be dissipated in the joint damper and the remainder in the two plates. Interest is focused on the ratios of these three energy dissipations to the power input by the external forcing, denoted by R_d, R_1 and R_2, respectively.

To begin with the spring stiffness is given the values 10^4 N (= Nm/rad/m), 10^6 N and 10^8 N, respectively, which leads to weak, transitional and strong coupling for the plates considered. The damper strength (in Nms/rad/m) is increased and the various energy receptances are plotted for a constant value of the driving frequency. It is noticed that for the weak spring of stiffness 10^4 N, the energy transferred to the undriven plate increases as the damper strength increases until it reaches a maximum constant level when the coupling becomes very strong. When the joint has a stiff spring of 10^8 N it is noted that

TABLE 1

Parameters used in the examples

Parameter	Plate one	Plate two	Units
Mass density (ρ)	78·0	78·0	kg/m^2
Length (L_x)	1·2	0·8	m
Width (L_y)	1·0	1·0	m
Rigidity (D)	$1{\cdot}923 \times 10^4$	$1{\cdot}923 \times 10^4$	Nm
Damping strength (c)	10·0	10·0	s^{-1}

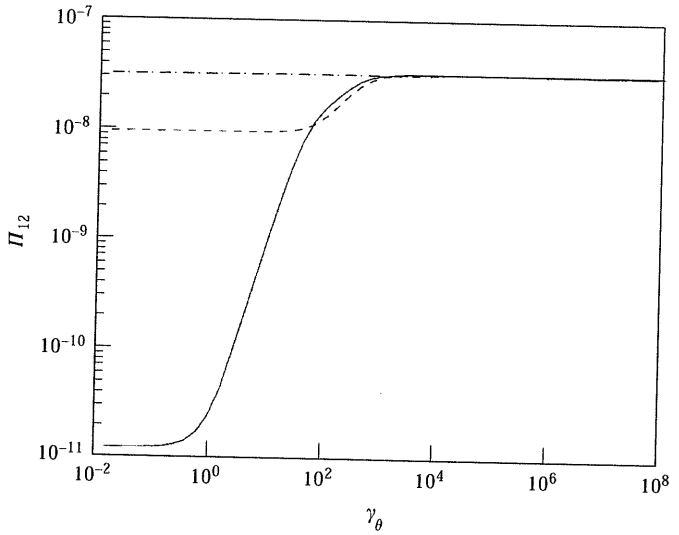

Figure 3. Variation in Π_{12} with γ_0 for $\omega = 10\,000$ rad/s for the case of two simply supported plates coupled through rotation: ——, $K_0 = 1 \times 10^4$ N; – – – –, $K_0 = 1 \times 10^6$ N; –·–·–·–·–·–, $K_0 = 1 \times 10^8$ N.

the energy transferred to plate two is at the limit level for a rigid coupling regardless of the damper strength, as shown in Figure 3.

The energy dissipated at the joint has a different pattern of changes. It is seen that the energy dissipated increases as the damper strength increases until it reaches a maximum level at a specific value of γ after which it falls again to minimum levels when the damper becomes very strong. This is to be expected since the damper is then blocked and unable to dissipate much energy. Maximum dissipation at the joint is thus related to a damping strength for which the overall joint strength is transitional between weak and strong. When

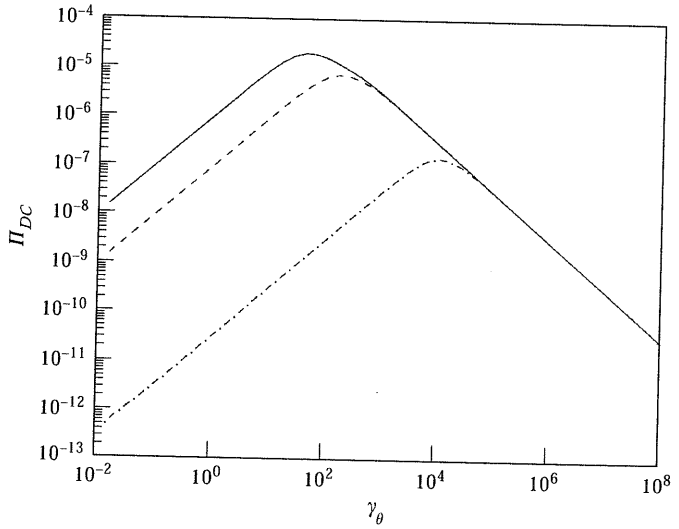

Figure 4. Variation in Π_{DC} with γ_0 for $\omega = 10\,000$ rad/s for the case of two simply supported plates coupled through rotation; key as per Figure 3.

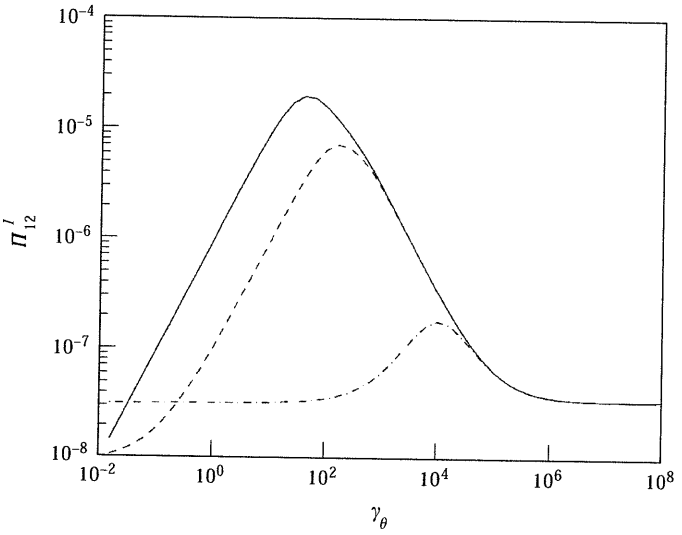

Figure 5. Variation in Π'_{12} with γ_θ for $\omega = 10\,000$ rad/s for the case of two simply supported plates coupled through rotation; key as per Figure 3.

the spring stiffness increases, it is seen that the energy dissipated at the joint will have the same pattern of changes, however, it is seen that in the case of a stiff spring, the maximum dissipation of energy at the joint is associated with a damper strength which is equal to $\gamma = K/\omega$, but the position of this maximum value decreases as the value of the spring stiffness increases, as shown in Figure 4.

The energy that leaves plate one increases as the damper strength increases and it reaches a maximum level at the value of damper strength for which the energy dissipation is also maximum. For this value of damping strength, the bulk of the energy leaving plate one is dissipated at the joint. As the joint damper strength increases further the energy that leaves plate one decreases until it reaches a constant level which represents the limit for the case of rigid joint. For this increased level of joint damping, most of the energy that leaves plate one is then transferred to plate two and is dissipated there. For the case of strong spring of stiffness 10^8 N, the energy that leaves plate one is at almost the same level, but it reaches a maximum level at a value associated with the maximum dissipation at the joint, as shown in Figure 5.

For the case of the weak spring, the input power also increases as the damping strength increases until it becomes maximum for a value of the damper strength which lies in the transitional region. As the damping increases, it falls rapidly and then remains at a constant low level for strong coupling. For the case of the strong spring of stiffness 10^8 N, the power input into the first plate is also at a constant level and does not show changes with the damper strength unlike the previous case. It is also found that the level of input power depends on the driving frequency.

Next, the ratios R_d, R_1 and R_2 are plotted in Figure 7 in order to gain some understanding of how these ratios change with the damper strength. For the case of a weak spring, it is seen that when the damper strength is weak, most of the input power is dissipated in the first plate, while the energy transferred through, and dissipated in, the damper are at minimum levels. As the damper strength increases, the energy dissipated in plate one drops until it reaches a minimum level for moderate coupling strength. The energy of plate two on the other hand increases as the coupling strength increases, as does

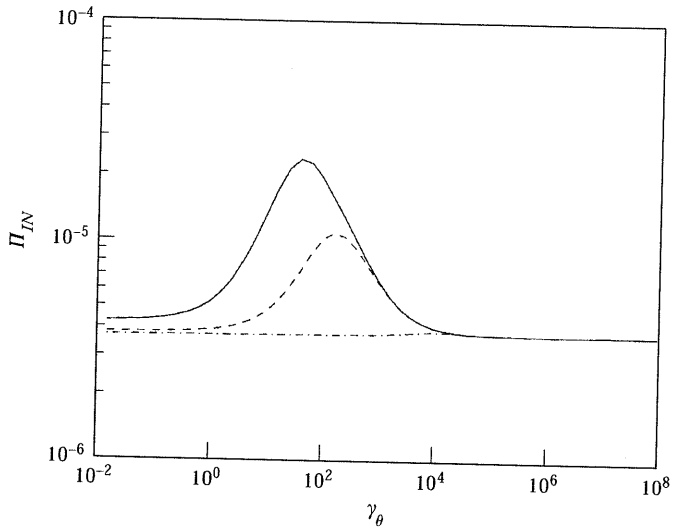

Figure 6. Variation in Π_{IN} with γ_0 for $\omega = 10\,000$ rad/s for the case of two simply supported plates coupled through rotation; key as per Figure 3.

the energy dissipated in the damper. It is seen that in this case the bulk of the input power is being dissipated in the damper with only a small percentage being dissipated in plates one and two. When the damper strength increases further, the ratio R_2 decreases as the damper becomes blocked while, on the other hand, R_d and R_1 increase again to reach constant levels for the limit of a rigid joint.

When the ratios R_d, R_1 and R_2 are plotted versus frequency for this case for different values of the damper strength, similar behaviour is noticed over a range of frequencies (see Figure 8). It is clear from the figure that the maximum dissipation of energy in the damper occurs for a damper strength which lies in the transitional region between weak and strong coupling.

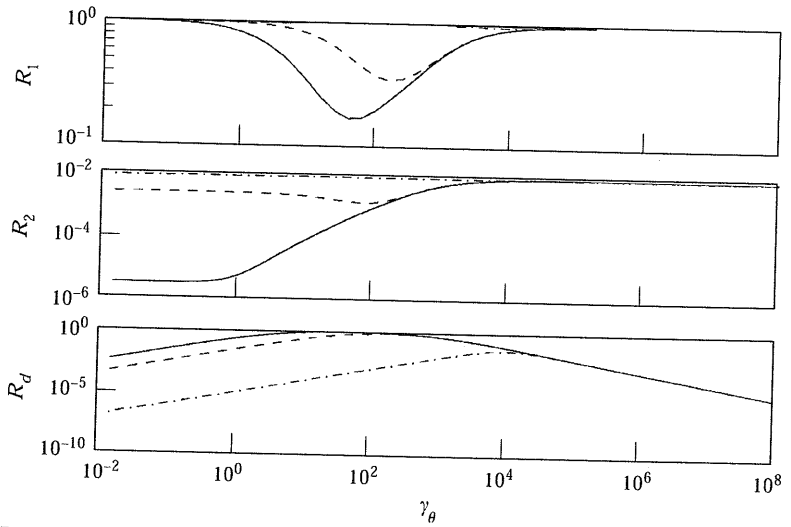

Figure 7. Variation in R_1, R_2 and R_d with γ_0 for $\omega = 10\,000$ rad/s for the case of two simply supported plates coupled through rotation; key as per Figure 3.

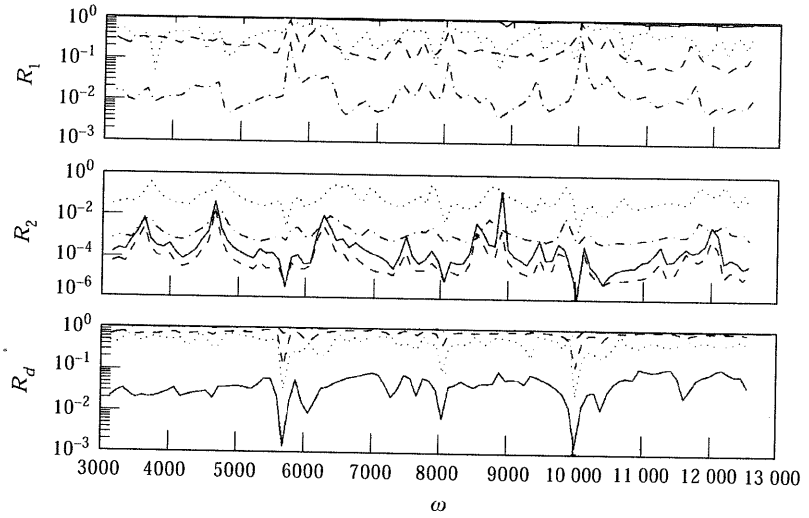

Figure 8. Variation in R_1, R_2 and R_d with ω for $K_0 = 10\,000$ N for the case of two simply supported plates coupled through rotation: ——, $\gamma_0 = 1 \times 10^{-2}$ Ns; – – – –, $\gamma_0 = 1$ Ns; –·–·–·–·–·–, $\gamma_0 = 1 \times 10^2$ Ns; ·····, $\gamma_0 = 1 \times 10^4$ Ns.

When the three ratios R_d,$R_1$and $R_2$are plotted for the case of a stiff spring, it is noticed that the ratio R_d has the same pattern of behaviour as before and reaches a maximum at $\gamma = K/\omega$ but is seen that this ratio is very small for all values of the damper strength, as might be expected since the damper is blocked by the very stiff spring. It follows that the power input is dissipated mostly in the plates. In this case, the ratios R_1 and R_2 remain at nearly constant levels for all values of the damper strength, which represents the limit for a rigid joint. This idea is confirmed when the ratios are plotted against frequency for different values of the damper strength (see Figure 9).

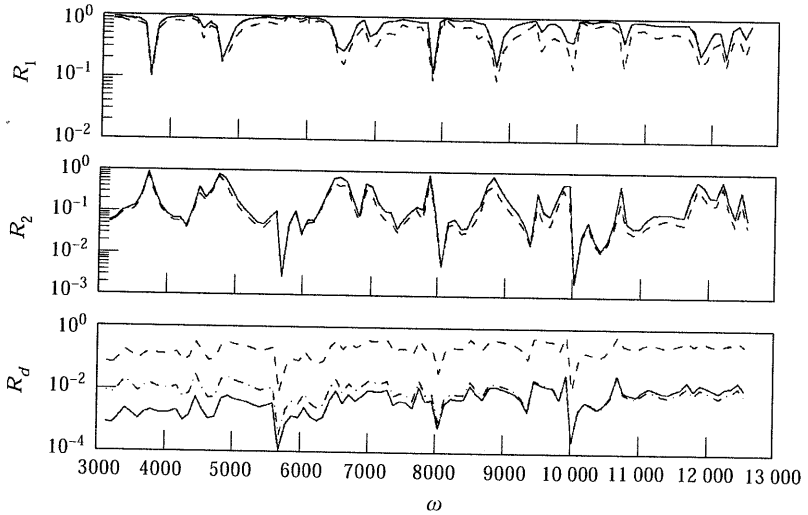

Figure 9. Variation in R_1, R_2 and R_d with ω for $K_0 = 10^8$ N for the case of two simply supported plates coupled through rotation: ——, $\gamma_0 = 1 \times 10^2$ Ns; – – – –, $\gamma_0 = 1 \times 10^4$ Ns; –·–·–·–·–·–, $\gamma_0 = 1 \times 10^6$ Ns.

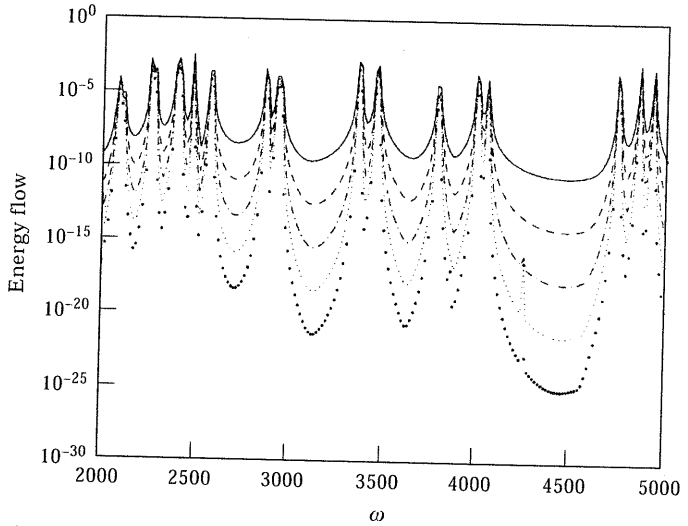

Figure 10. Variation in the energy flow through the joints in a row of six plates for $K_y = 10^6$ N m^{-2} amd $K_0 = 10^2$ N and light internal damping in the plates: ——, joint 1; – – –, joint 2; —·—·—·—, joint 3; ....., joint 4; . . . . . , joint 5.

Lastly, it should be noted that the summations over the transverse modal components used in the various energy receptances expressions need only a small number of modes to converge. For the examples presented here, it was found that 10 modes were enough to guarantee convergence in the frequency band of interest for the examples given.

9.2. SIX PLATES

In the second set of examples, a row of six identical plates is considered, with the first plate driven by a point force. The properties of the plates are the same as given for plate

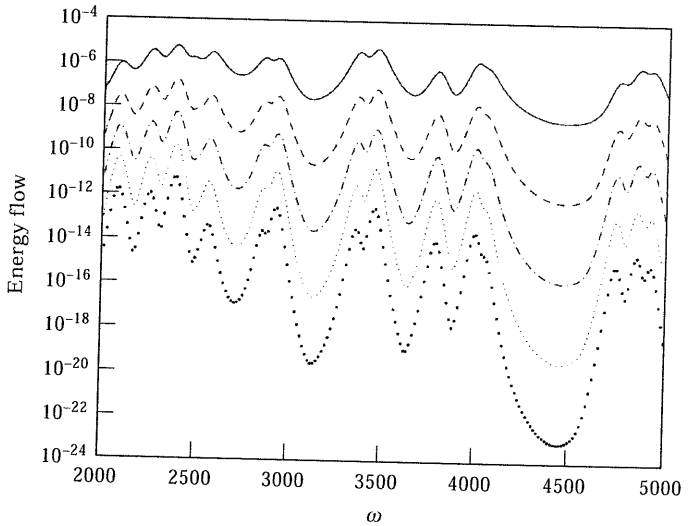

Figure 11. Variation in the energy flow through the joints in a row of six plates for $K_y = 10^6$ N m^{-2} and $K_0 = 10^2$ N and heavy internal damping in the plates; key as per Figure 10.

TABLE 2

Damping distributions considered in the examples

Case no.	γ_1	γ_2	γ_3	γ_4	γ_5
1	γ	0	0	0	0
2	0	γ	0	0	0
3	0	0	γ	0	0
4	0	0	0	γ	0
5	0	0	0	0	γ
6	$0{\cdot}5\gamma$	$0{\cdot}5\gamma$	0	0	0
7	$0{\cdot}5\gamma$	0	0	0	$0{\cdot}5\gamma$
8	$0{\cdot}2\gamma$	$0{\cdot}2\gamma$	$0{\cdot}2\gamma$	$0{\cdot}2\gamma$	$0{\cdot}2\gamma$
9	$0{\cdot}6\gamma$	$0{\cdot}1\gamma$	$0{\cdot}1\gamma$	$0{\cdot}1\gamma$	$0{\cdot}1\gamma$

one in Table 1. Figure 10 shows the energy that is transferred through each joint for the case of weak and conservative coupling. It is seen that the energy is lost through the internal damping as the energy flows through the plates of the panel. It can also be seen that resonant transmission occurs at some frequencies which is characterized by sharp increases in the energy flow (the beginning of "stop" and "pass" band behaviour is apparent).

When the damping in the individual plates becomes heavy, it is seen that the plots become smoother than those in Figure 10 and the spikes which occur at resonance are eliminated (see Figure 11). The energy levels of the various plates also decrease as the energy travels from the driven plate through the panel.

Next, a row of plates is considered where the joints have compliance in rotation only. The first plate is driven by a point force and the joints are damped in a variety of ways by distributing the same total amount of damping γ over the joints in different proportions (see Table 2). Here the ratio R_d denotes the ratio of the total energy dissipated due to

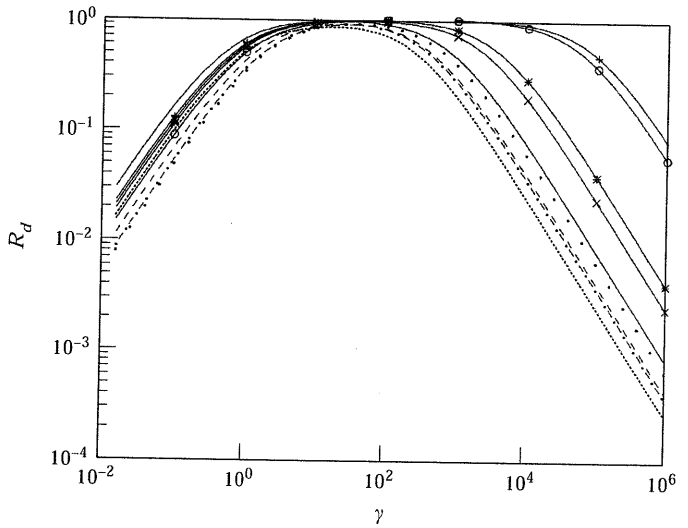

Figure 12. Variation in R_d with γ in a row of six identical plates for $K_y = 10^{10}$ N m^{-2} and $K_\theta = 10^2$ N in all joints and light internal damping in the plates: ——, case 1; – – –, case 2; ....., case 3; –·–·–·–·–, case 4; · · · · ·, case 5; —×—, case 6; —*—, case 7; —○—, case 8; —+—, case 9.

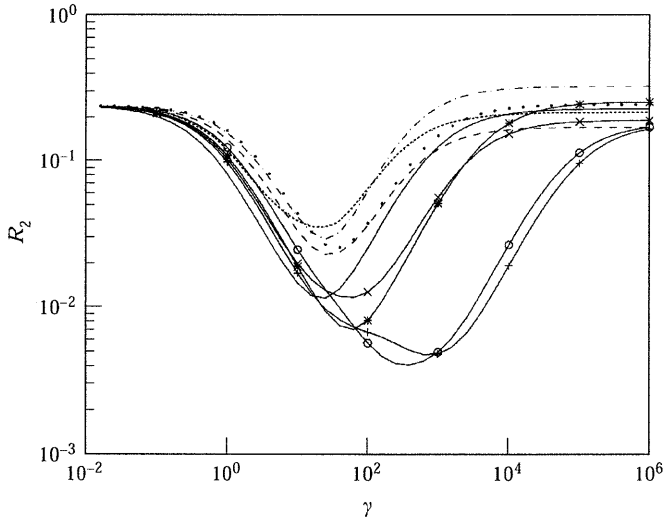

Figure 13. Variation in R_2 with γ in a row of six identical plates for $K_y = 10^{10}$ N m^{-2} and $K_\theta = 10^2$ Nms in all joints and light internal damping in the plates; key as per Figure 12.

coupling damping in all joints to the power input by the external forcing. The ratio R_n denotes the ratio of the energy dissipated in plate n to the total input power (i.e., R_2 measures the energy dissipated in the second plate and R_6 that in the sixth plate). Figures 12–14 show R_d, R_2 and R_6 plotted for increasing values of γ for the cases shown in Table 2 above. It is seen that for each case, the dissipation of energy is maximized at a particular value of the damper strength. Moreover, it is seen that for some, relatively

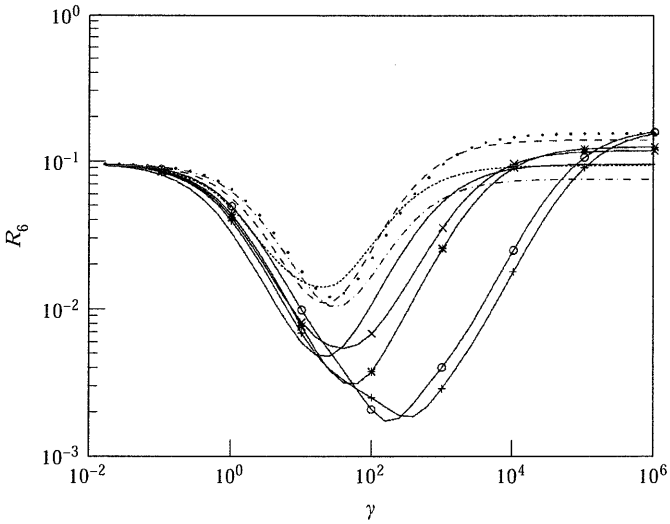

Figure 14. Variation in R_6 with γ in a row of six identical plates for $K_y = 10^{10}$ N m^{-2} and $K_\theta = 10^2$ N in all joints and light internal damping in the plates; key as per Figure 12.

high values of γ, the greatest degree of power dissipation in the joints is achieved by distributing the damping throughout the structure, while for lesser amount of damping a more significant effect is achieved by inserting all the available damping in the joint nearest the drive point. Additionally, it is never worthwhile concentrating the damping wholly in the second, third, fourth or fifth joints. No doubt the best distribution of damping between the joints could be sought by optimization. It is also worth noting that when the coupling between plates is stiff, the damping in the joints has no effect on the ratio R_n in the plates, since the ratio of the energy dissipated in the damper is then very small, regardless of the damper strength.

10. CONCLUDING REMARKS

A receptance approach has been presented for the analysis of energy flows and energy levels in thin rectangular plates coupled together by compliant and dissipative joints. The main purpose of the analysis presented is to examine the effects of including damping in the joints on the various energy receptances of the system. It is shown that joint damping is most effective when the couplings are not very strong and that for any combination of joints and total quantity of damping, there will be a particular distribution of the damping for which the bulk of the input power is dissipated in the joints, minimizing the energy levels in the unforced plates. For the case of a row of plates coupled together, coupling damping is seen to be most effective either when it is relatively evenly distributed among all the joints or, alternatively, placed wholly in the joint nearest the drive point, depending on the precise strengths of the coupling elements.

REFERENCES

1. R. VAICAITIS, F. W. GROSVELD and J. S. MIXSON 1985 *American Institute of Aeronautics and Astronautics Journal of Aircraft* **22**, 303–310. Noise transmission through aircraft panels.
2. B. M. GIBBS and C. L. S. GILFORD 1976 *Journal of Sound and Vibration* **49**, 267–286. The use of power flow methods for the assessment of sound transmission in building structures.
3. P. G. CRAVEN and B. M. GIBBS 1981 *Journal of Sound and Vibration* **77**, 417–427. Sound transmission and mode coupling at junctions of thin plates, part I: representation of the problem.
4. B. A. T. PETERSSON, C. PIERRE and E. H. DOWELL 1987 *Journal of Sound and Vibration* **114**, 549–564. Localization of vibrations by structural irregularity.
5. L. CREMER, M. HECKL and E. E. UNGAR 1988 *Structure Borne Sound* Berlin: Springer Verlag; second-edition.
6. J. L. GUYADER, C. BOISSON and C. LESUEUR 1982 *Journal of Sound and Vibration* **81**, 81–92. Energy transmission in finite coupled plates, part I: theory.
7. Y. SHEN and B. M. GIBBS 1986 *Journal of Sound Vibration* **105**, 73–90. An approximate solution for the bending vibration of a combination of thin rectangular plates.
8. R. S. LANGLEY 1989 *Journal of Sound and Vibration* **135**, 319–331. Application of the dynamic stiffness method to the free and forced vibrations of aircraft panels.
9. A. N. BERCIN and R. S. LANGLEY 1996 *Computers and Structures* **59**, 869–875. Application of the dynamic stiffness technique to the in-plane vibrations of plate structures.
10. J. M. CUSCHIERI 1990 *Journal of the Acoustical Society of America* **87**, 1159–1165. Structural power flow analysis using a mobility approach of an L-shaped plate.
11. J. M. CUSCHIERI 1992 *Journal of the Acoustical Society of America* **91**, 2686–2695. Parametric analysis of the power flow on an L-shaped plate using a mobility power flow approach.
12. C. SIMMONS 1991 *Journal of Sound and Vibration* **144**, 215–227. Structure borne sound transmission through plate junctions and estimates of SEA coupling loss factors using the Finite Element Method.
13. S. AZIMI, J. F. HAMILTON and W. SOEDEL 1984 *Journal of Sound and Vibration* **93**, 9–29. The receptance method applied to the free vibration of continuous rectangular plates.

14. E. K. DIMITRIADIS and A. D. PIERCE 1988 *Journal of Sound and Vibration* **123**, 497–412. Analytical solution for the power exchange between strongly coupled plates under random excitation: a test of statistical energy analysis concepts.
15. C. R. FREDO 1995 *Ph.D. Thesis, Chalmers Institute of Technology, Sweden*. Statistical energy analysis and the individual case.
16. HYUN-SIL KIM, HYUN-JOO KANG and JAE-SEUNG KIM 1994 *Journal of the Acoustical Society of America* **96**, 1557–1562. Transmission of bending waves in inter-connected rectangular plates.
17. M. BESHARA, G. Y. CHOHAM, A. J. KEANE and W. G. PRICE 1997 in *Statistical Energy Analysis: An Overview with Applications in Structural Dynamics* (A. J. Keane and W. G. Price, editors) 113–139. Cambridge University Press. Statistical energy analysis of nonconservative systems.
18. M. BESHARA and A. J. KEANE 1997 *Journal of Sound and Vibration* **203**, 321–339. Vibrational energy flows in beam networks with compliant and dissipative joints.

APPENDIX: NOMENCLATURE

A, B	left and right hand edges of a subsection
D	subsection rigidity
E	Young's modulus
F	modal component of external forcing
G	Green function
H	frequency response function of a mode of a subsection
K	stiffness per unit of length
L_{xn}, L_y	dimensions of subsections, see Figures 1 and 2
M	coupling moment
N	total number of joints in the system
S	cross-spectral density
T	period of oscillation
W	modal component of the Fourier transform of deflection
a	subsection area
c	viscous damping coefficient
f	excitation force
h	subsection thickness
i	number of half sine waves in x direction
j	number of half sine waves in y direction
k	dummy summation counter
m	mass
n	subsection counter in the x direction
v	velocity
x, y	rectangular co-ordinates
$\Delta_j(\omega)$	$1 + \Omega(G_{1,j_{00}}(0, 0, \omega) + G_{2,j_{00}}(0, 0, \omega))$
Π	spectral density of energy flow
Ψ	mode shape variation in the x direction
Φ	mode shape variation in the y direction
Ω	complex rotational stiffness per unit of length
γ	damping per unit of length
θ	plate rotation
ν	Poisson's ratio
ρ	mass per unit area
ω	radian frequency of oscillation.